第37卷 第2期 焊 接 学 报 Vol. 37 No. 2
2016年2月 TRANSACTIONS OF THE CHINA WELDING INSTITUTION February 2016

基于蒙特卡罗方法的铝/钢熔钎焊界面金属间化合物层生长分析

刘 宁[1,2]， 黄健康[1]， 陈满骄[1]， 石 玗[1]， 曹 睿[1*]

(1. 兰州理工大学 省部共建有色金属先进加工与再利用国家重点实验室，兰州 730050;
2. 宝钢集团新疆八一钢铁股份有限公司，乌鲁木齐 830022)

摘 要：针对铝/钢熔钎焊界面金属间化合物在SEM，EDS，XRD界面测试研究的基础上，确立了界面由Fe_2Al_5、$FeAl_3$等金属间化合物组成. 在此基础上采用蒙特卡罗方法(monte carlo method，MC)，建立了铝/钢界面铝、铁原子的扩散及Al-Fe金属间化合物生长模型，并进行了数值分析和对比研究进一步分析了金属间化合物的生长过程. 结果表明，所建立的模型能够很好地反映钢侧Fe_2Al_5的生长，铝侧$FeAl_3$离散存在，且金属间化合物层的厚度接近试验测量结果.

关键词：铝钢界面； 金属间化合物； 蒙特卡罗； 生长分析

中图分类号：TG 457 **文献标识码**：A **文章编号**：0253－360X(2016)02－0055－04

0 序 言

铝/钢异种金属的复合结构能够同时满足轻量化和结构性能的双重要求，因此铝/钢异种金属的连接受到了人们的广泛关注[1]. 铝、钢两种金属的物理、化学性能相差较大，焊接时极易产生大量Fe_2Al_5，$FeAl_3$等脆硬性金属间化合物，从而严重降低焊接接头的力学性能[2-4]. 铝/钢界面处，Fe_2Al_5，$FeAl_3$等金属间化合物不同的生长方式，导致了其微观形貌及界面层厚度的不同[5]. 而脆性金属间化合物对铝/钢接头力学性能的影响程度与其成分、形貌特征、分布状态及生长方式有关，因此通过研究铝/钢焊接接头界面金属间化合物的微观组织分布和形成过程，以实现对界面金属间化合物生长的控制，从而获得符合性能要求的铝/钢焊接接头.

对于异种金属焊接的数值模拟，大多集中在温度场及应力应变等方面[6,7]，文中首次将蒙特卡罗方法应用于铝/钢异种金属界面化合物层微观组织形成生长过程，通过对脉冲旁路耦合电弧MIG熔钎焊铝/钢接头界面微观组织的分析，建立了铝/钢界面金属间化合物的生长模型. 对其微观组织形成及生长过程进行数值计算，并对金属间化合物层厚度进行对比分析，以进一步分析化合物层的生长机理.

收稿日期：2014－05－08
基金项目：国家自然科学基金资助项目(51165023)
* 参加此项研究工作的还有兰州理工大学陈剑虹

1 铝/钢界面金属间化合物

1.1 铝/钢接头的获取

脉冲旁路耦合电弧MIG焊能很好的对母材的热输入进行控制，进而有效控制界面区金属间化合物的生成. 故文中通过脉冲旁路耦合电弧MIG焊，采用直径为1.2 mm的ER5356铝合金焊丝，在厚度为2 mm、每平方米面积含锌100 g的镀锌钢板(基体为Q235低碳钢)上进行平板堆焊试验. 对试验所得焊接接头试样采用0.5% HF溶液进行腐蚀. 利用MEF3大型光学显微镜和JSM-5600LV低真空扫描电子显微镜观察铝/镀锌钢板脉冲旁路耦合电弧MIG熔钎焊连接界面区的组织形貌以及金属间化合物，并进行线扫描、能谱区域扫描观察和分析，对接头界面进行XRD分析.

表1 ER5356铝合金焊丝的化学成分(质量分数，%)

Table 1 Chemical compositions of ER5356

Mg	Cr	Si	Cu	Zn	Mn	Ti	Al
5.00	0.10	0.30	0.05	0.05	0.15	0.01	余量

1.2 界面化合物分析

对铝/钢熔钎焊焊接接头试样采用SEM观察其界面微观组织，其微观组织形貌如图1所示. 由图1可知在铝与镀锌钢板之间，生成了包含两层且厚度小于10 μm的金属间化合物过渡层. 靠近铝侧，化

(C)1994-2019 China Academic Journal Electronic Publishing House. All rights reserved. http://www.cnki.net

合物呈针状或絮状向铝侧生长;而靠近镀锌钢侧的化合物以舌状或条状向镀锌钢侧生长. 为了确定界面微观组织的物相,对界面显微组织进行线扫描,结果如图2所示,Fe元素含量垂直于结合面从钢侧向铝侧不断下降,而Al元素含量则上升,在界面化合物层处,Al,Fe元素含量较为均匀,元素含量曲线近似出现平台,说明接头界面反应层的物质应为铝铁金属间化合物. 图3为点扫描区域图,为了更进一步确定铝/镀锌钢板熔钎焊接头界面化合物相的成分,分别对图3中的A,B区域进行EDS能谱分析,以确定各反应层中的元素比例,其结果如表2所示.

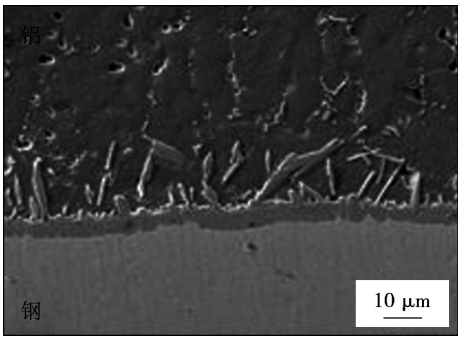

图1 铝与镀锌钢板熔钎焊的界面微观组织

Fig. 1 Interfacial microstructures of cross-section by aluminum-galvanized steel welding-brazing

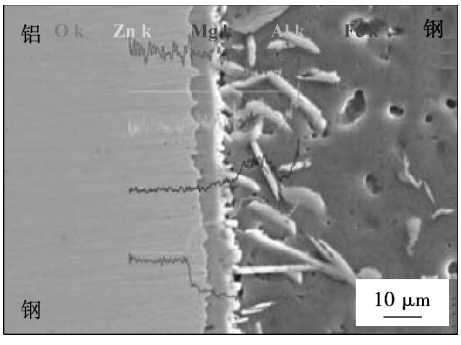

图2 界面显微组织及线扫描

Fig. 2 Microstructure and line scanning of interface

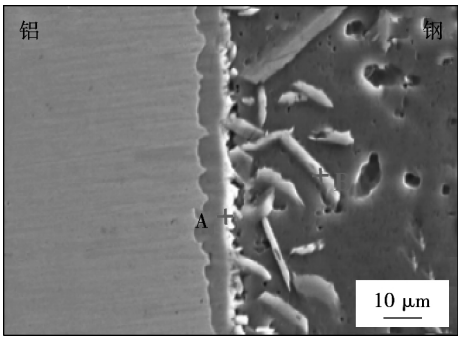

图3 界面处不同区域的EDS分析

Fig. 3 EDS analysis of different areas of interface

根据表2中结果可知A区域中的Fe,Al原子个数比接近1:3,表明A区域中的成分是$FeAl_3$. 而B区域中的Fe,Al原子个数比接近2:5,表明B区域中的成分为Fe_2Al_5. 并对焊缝接头界面做XRD分析,其结果如图4所示. 从图4可以看出,界面金属间化合物主要有Fe_2Al_5,$FeAl_3$,而Al_2Mg,$Al_{0.7}Fe_3Si_{0.3}$等化合物的存在可能是由于母材或焊丝成分所导致的.

表2 界面处不同区域的成分

Table 2 Compositions of different areas of interface

区域	质量分数 ω(%)		原子分数 a(%)	
	Fe	Al	Fe	Al
A	39.97	56.00	23.94	69.42
B	23.72	68.97	32.72	76.54

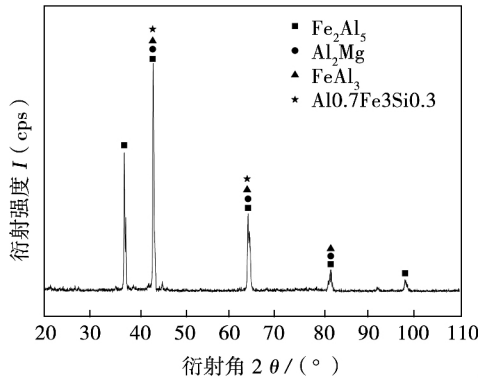

图4 铝钢界面层的XRD分析

Fig. 4 XRD analysis of joint interface

由EDS能谱分析及XRD分析结果可以确定,在铝/镀锌钢板熔钎焊焊接界面处形成的化合物主要是Fe_2Al_5和$FeAl_3$.

2 基于蒙特卡罗的铝/钢界面化合物生长分析

2.1 铝钢界面MC过程

蒙特卡罗方法可以直接显示材料的微观结构及其演化过程. 在蒙特卡罗方法模拟过程中,将微观结构映射到一个离散的二维方格系统中,每一个网格赋予一个介于$1 \sim Q$间的随机值,表示晶粒的取向,其中Q表示系统中所有可能的晶粒取向. 一个晶粒内的所有网格都具有相同的取向值,相邻的两个不同取向值的网格连接处为晶界. MC模拟晶粒生长的步骤如下. (1) 对计算的对象进行网格划分$N \times N$. (2) 对每个网格赋予一个从$1 \sim Q$的值,确定该点的晶粒取向. (3) 判断相邻网格的取向是否

(C)1994-2019 China Academic Journal Electronic Publishing House. All rights reserved. http://www.cnki.net

相同,若相同则属于相同晶粒,反之则处于晶界位置. (4) 计算转变后的能量变化,若 $\Delta E<0$,新取向被接受. 界面能是晶粒取向差的函数,表达式为

$$E = -\sum_{ij} MS_iS_j \tag{1}$$

式中: S_i,S_j 为晶粒取向值,从 $1 \sim Q$ 中选取. 矩阵 M_{ij} 为

$$M_{ij} = J(1-\delta_{ij}) \tag{2}$$

式中: J 为单位面积自由能; δ_{ij} 为 Kronecker δ 函数.

在铝/钢接头界面金属间化合物层微观组织模拟过程中,由于界面层厚度在 10 μm 左右,模拟的区域相对较小,故在模型中假定晶粒生长过程温度是一定的. 且铝/钢界面层微观组织的模拟系统是两种不同属性单元,因此对波茨模型进行了改进. 对模型的改进主要包括以下 3 点: (1) 设定 0,1 两个不同的初始状态,分别用来区分铝侧和钢侧. (2) 在计算能量时,将生成的相作为一个单元来计算能量的减少. (3) 根据试验确定相成分的方法,按原子比对化合物的成分进行标定.

对能量采用 6 × 7 的网格单元进行统计,且能量统计的数学表达式为

$$E_{\mathrm{mcs}} = \sum_{j=0}^{n1}\sum_{i=0}^{n2} E_{\mathrm{nergy}}(i,j) \tag{3}$$

$$E_{\mathrm{nergy}} = \begin{cases} -100 & L_{\mathrm{V}} = 30 \\ -60 & L_{\mathrm{V}} = 32 \end{cases} \tag{4}$$

式中: E_{mcs} 为蒙特卡罗步所对应的网格能量值; mcs 为蒙特卡罗时间步长; $E_{\mathrm{nergy}}(i,j)$ 为统计区域的能量值; L_{V} 为统计区域的铝原子个数.

2.2　蒙特卡罗数值分析

在铝/钢熔钎焊界面的几何模型中,采用网格大小为 525 × 450,设定每个网格长度为 1 μm. 根据试验结果可知,铝/钢界面金属间化合物层主要由 Fe_2Al_5,$FeAl_3$ 组成,故在模拟系统中将网格分为铝和铁两部分,其中 $Q=1$ 侧为铝,$Q=0$ 侧为铁. 实际铝/钢焊接过程中,Al,Fe 原子之间发生互扩散,在模型中加以简化,仅考虑铝向钢侧的扩散,且铝向钢中的扩散能力随着距铝/钢界面的间距的增加而减弱,在文中预设了铝在钢中扩散的概率分布,其数学表达式为

$$P = 0.9^n \quad (0 \leqslant n \leqslant N) \tag{5}$$

式中: n 为距界面的距离; N 为到界面的最大距离.

铝/钢熔钎焊焊接界面区主要成分为 Fe_2Al_5 和 $FeAl_3$,在此模型中忽略组分比较少的其它化合物相,仅考虑主要相 Fe_2Al_5 和 $FeAl_3$. 系统中初设一能量值,焊接过程中随着扩散过程进行及化合物的形成,体系的能量逐渐减小.

能量统计遵从以下三个原则: (1) 统计区域内的网格比即为原子比. (2) 统计区域内原子比满足 Fe∶Al = 2∶5,表明该区域生成的金属间化合物为 Fe_2Al_5,设定此时系统能量降低 100. (3) 若统计区域原子比满足 Fe∶Al = 1∶3,表明该区生成物为 $FeAl_3$,此时系统能量降低 60.

石玗等人[8] 认为在 Fe-Al 化合物形成过程中,形成 Fe_2Al_5 自由能变化大于形成 $FeAl_3$ 自由能的变化. 文中取 -100、-60 这两个相对折算值来表示形成不同相时自由能的变化快慢的趋势.

在此模型中采用式(3)、式(4) 对 Al,Fe 原子扩散生长过程的能量进行统计,图 5 为统计区域的能量变化曲线,随着整个扩散过程的进行,系统的能量不断减小,符合晶粒生长蒙特卡罗方法基于能量最小的原则.

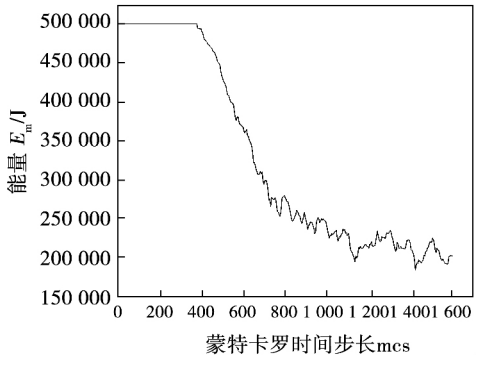

图 5　能量变化曲线

Fig. 5　Curves of energy

扩散过程结束后,对金属间化合物的成分进行标定. 采用 3 × 3 的单元对 Fe_2Al_5 进行标定,在这个小单元中若 Al 原子数为 5,则此单元为 Fe_2Al_5; 在 2 × 2 的小单元中标定 $FeAl_3$,Al 原子个数为 3,则此单元为 $FeAl_3$,并对化合物层的厚度进行统计. 对式(3) 控制的扩散后的系统通过以上两种原子比确定成分的方法对各相进行标定,可得铝/钢界面化合物层微观组织模拟结果. 图 6 为不同蒙特卡罗时间步长的界面化合物层模拟结果,可以看出随模拟时间增长,化合物层厚度明显增加.

2.3　结果对比分析

图 7 为铝/钢熔钎焊焊接接头金属间化合物层微观形貌的模拟和试验结果,图 7a 为试验结果,图 7b 为模拟温度为 800 ℃ 时的模拟结果. 由图 7b 模拟结果可以看出,金属间化合物包含两层,靠近钢的一侧形成连续分布的 Fe_2Al_5,而 $FeAl_3$ 则离散的分布在铝侧. 与试验结果进行对比,模拟结果与试验结果吻合较好,同时也证明了模型的可行性. 对化合物层的厚度进行统计,可得厚度约为 9 μm,试验中所

(C)1994-2019 China Academic Journal Electronic Publishing House. All rights reserved.　http://www.cnki.net

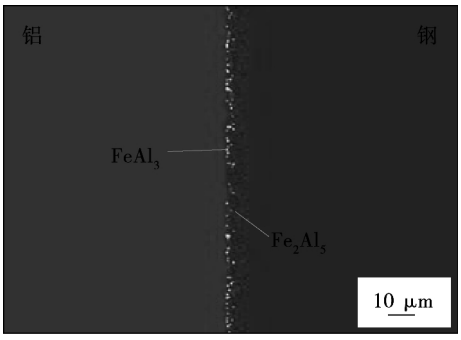

(a) 500 mcs

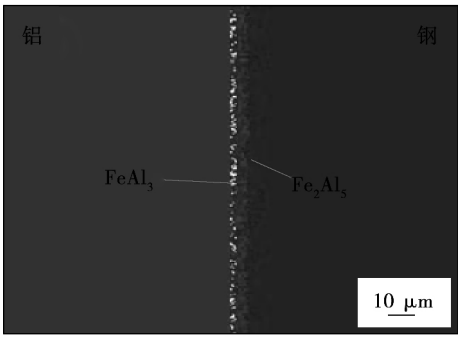

(b) 1 000 mcs

图 6 不同 mcs 界面层微观组织模拟结果

Fig. 6 Simulated microstructure of aluminum steel joint at different mcs

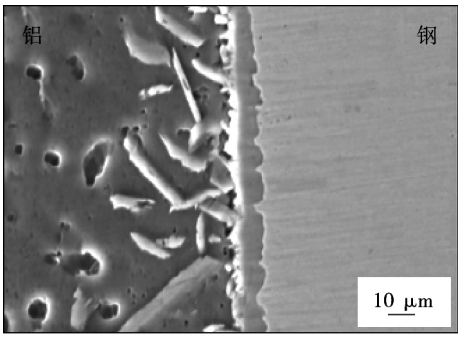

(a) 试验结果

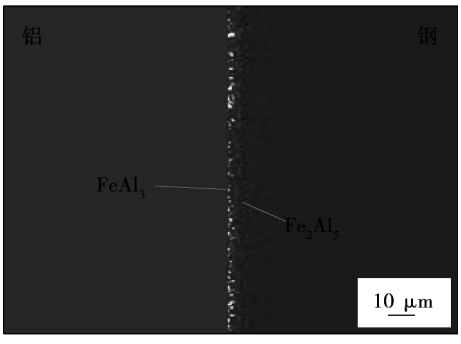

(b) 模拟结果

图 7 铝/钢界面层微观组织形貌

Fig. 7 Microstructure morphology of aluminum steel joint

得化合物层厚度小于 10 μm，模拟结果与试验结果进行比较吻合较好.

3 结 论

(1) 通过线扫描、区域能谱分析、XRD 分析，发现铝/钢界面层是由 Fe_2Al_5、$FeAl_3$ 等 Al-Fe 化合物组成.

(2) 通过试验对比验证，所建立的铝/钢界面蒙特卡罗生长模型是正确的，Fe_2Al_5、$FeAl_3$ 在界面层形成，且数值分析所得的金属间化合物层的厚度接近试验的测量值.

参考文献:

[1] 石常亮，何 鹏，冯吉才，等. 铝/镀锌钢板 CMT 熔钎焊界面区组织与接头性能[J]. 焊接学报，2006，27(12)：61－64.
Shi Changliang，He Peng，Feng Jicai，*et al*. Interface microstructure and mechanical property of CMT welding brazed joint between aluminum and galvanized steel sheet [J]. Transactions of China Welding Institution，2006，27(12)：61－64.

[2] Zhang J X，Chandl R S，Chen Y Z，*et al*. Effect of residual stress on the strength of an alumina-steel joint by partial transient liguid phase (PTLP) brazing [J]. Journal of Materials Processing Technology，2002，122(2/3)：220－225.

[3] Alexandre M，Rajashekar S，Alexis D，*et al*. Dissimilar material joining using laser (aluminum to steel using zinc-based filler wire) [J]. Optics & Laser Technology，2007，39：652－661.

[4] 何 鹏，冯吉才，钱乙余. 接触反应法解决铝/不锈钢钎焊的缺陷及脆性[J]. 材料科学与工艺，2005，13(1)：82－85.
He Peng，Feng Jicai，Qian Yiyu. Resolve of fragile and defect problem for a new contect reaction brazing aluminum to stainless steel [J]. Materials Science and Technology，2005，13(1)：82－85.

[5] Shi Y，Shao L，Huang J K，*et al*. Effects of Si and Mg elements on microstructure of aluminum-steel joints produced by pulsed DE-GMA welding-brazing [J]. Materials Science and Technology，2013，29(9)：1118－1124.

[6] 赵洪运，舒凤远，张洪涛，等. 基于生死单元的激光熔覆温度场数值模拟[J]. 焊接学报，2010，31(5)：81－84.
Zhao Hongyun，Shu Fengyuan，Zhang Hongtao，*et al*. Numerical simulation on temperature field of laser cladding based on brith-death element method [J]. Transactions of China Welding Institution，2010，31(5)：81－84.

[7] 何 鹏，冯吉才，钱乙余. 异种材料扩散连接接头残余应力的分布特征及中间层的作用[J]. 焊接学报，2002，23(1)：76－80.
He Peng，Feng Jicai，Qian Yiyu. Distributions of residual stresses in diffusion bond of dissimilar ma-terials and effect of interlaye [J]. Transactions of China Welding Institution，2002，23(1)：76－80.

[8] 石 玗，何翠翠，黄健康，等. 铝钢焊接界面金属间化合物形成的热力学分析[J]. 兰州理工大学学报，2013，39(4)：5－7.

[下转第 62 页]

(C)1994-2019 China Academic Journal Electronic Publishing House. All rights reserved. http://www.cnki.net

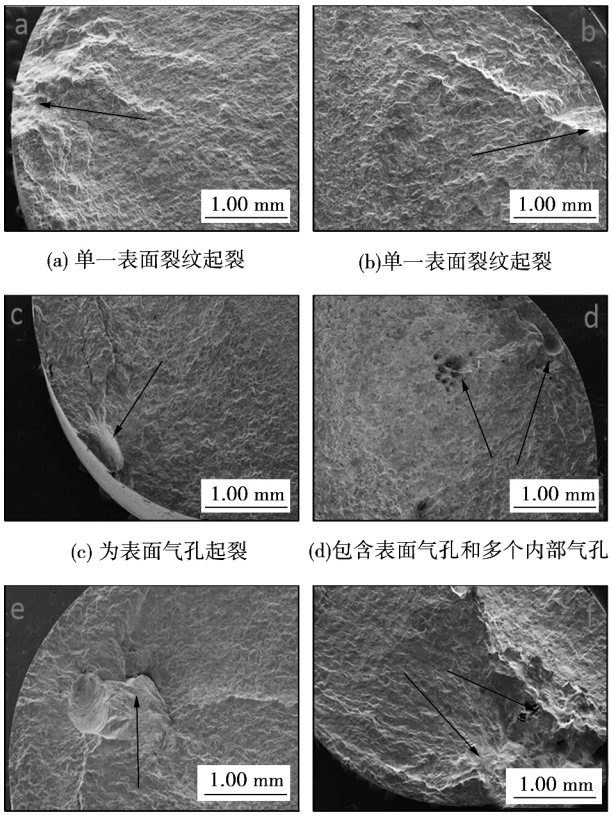

(a) 单一表面裂纹起裂 (b)单一表面裂纹起裂

(c) 为表面气孔起裂 (d)包含表面气孔和多个内部气孔

(e) 未融合 (f)表面裂纹和气孔 (箭头指向焊接缺陷处)

图5 焊接接头断口形貌

Fig. 5 Fracture morphology of welded joint

4 结 论

(1) 超声疲劳试验得到5A06母材试件,无余高焊接接头试件以及薄板对接接头试件的超声疲劳S-N曲线. 母材试件和两种焊接接头试件的超声疲劳S-N曲线在载荷循环周次超过10^7后,呈持续下降趋势,试件依然发生疲劳断裂,不存在疲劳极限. 焊接接头的疲劳性能较母材的疲劳性能差.

(2) 在$N=1\times10^7$循环次数下,圆柱状焊接接头试件和薄板状焊接接头试件的疲劳强度分别为母材试件疲劳强度的67.6%和62.5%;在$N=1\times10^9$循环次数下,圆柱状焊接接头试件和薄板状焊接接头试件的疲劳强度分别为母材试件疲劳强度的59.7%和51.3%.

(3) 在扫描电子显微镜下可以观察到母材的断口比较平整,有明显的疲劳辉纹特征. 而焊接接头的断口比较粗糙,存在气孔、未熔合等焊接缺陷导致焊接接头疲劳性能较母材低.

参考文献:

[1] Zettl B, Mayer H, Ede C, *et al*. Very high cycle fatigue of normalized carbon steels [J]. International Journal of Fatigue, 2006, 28(11): 1583-1589.

[2] Wang Q Y, Kawagoishi N, Chen Q. Fatigue and fracture behaviour of structural Al-alloys up to very long life regimes [J]. International Journal of Fatigue, 2006, 28(11): 1572-1576.

[3] Tanaka K, Akiniwa Y. Fatigue crack propagation behaviour derived from S-N data in very high cycle regime [J]. Fatigue & Fracture of Engineering Materials & Structures, 2002, 25(8/9): 775-784.

[4] 何 超, 崔仕明, 刘永杰, 等. 气孔对铝合金焊接接头超长疲劳寿命的影响 [J]. 焊接学报, 2014, 35(11): 18-22.
He Chao, Cui Shiming, Liu Yongjie, *et al*. Effect of pore on super long fatigue life of aluminum alloy welded joint [J]. Transactions of the China Welding Institution, 2014, 35(11): 18-22.

[5] 吴良晨,王东坡, 邓彩艳, 等. 超长寿命区间16Mn钢焊接接头疲劳性能 [J]. 焊接学报, 2008, 29(3): 117-120.
Wu Liangchen, Wang Dongpo, Deng Caiyan, *et al*. Fatigue properties of welded joints of 16Mn steel in super long life region [J]. Transactions of the China Welding Institution, 2008, 29(3): 117-120.

[6] Bathias C. Piezoelectric fatigue testing machines and devices [J]. International journal of fatigue, 2006, 28(11): 1438-1445.

[7] 吴良晨. 超声频分量双周疲劳载荷作用下焊接接头的疲劳性能 [D]. 天津大学, 2008.

作者简介: 李 想,男,1989年出生,硕士. 主要从事超长寿命区间内疲劳寿命方面的研究. Email: li_xiang_tju@163.com

通讯作者: 龚宝明,男,博士,讲师. Email: gong_bm@tju.edu.cn

[上接第58页]

Shi Yu, He Cuicui, Huang Jiankang, *et al*. Thermodynamic analysis of the forming of intermetallic compounds on aluminum-steel welding interface [J]. Journal of Lanzhou University of Technology, 2013, 39(4): 5-7.

作者简介: 刘 宁,女,1989年出生,硕士研究生. 从事铝/钢熔钎焊焊接界面行为研究. Email: o0oliuning@126.com

通讯作者: 黄健康,男,副教授,硕士研究生导师. Email: sr2810@163.com

(C)1994-2019 China Academic Journal Electronic Publishing House. All rights reserved. http://www.cnki.net

Oxygen distribution and numerical simulation of weld pool profiles during arc assisted activating TIG welding FAN Ding[1], HUANG Zicheng[1], HUANG Jiankang[1,2], HAO Zhenni[1,3], WANG Xinxin[1], HUANG Yong[1] (1. School of Materials Science and Engineering Lanzhou University of Technology, Lanzhou 730050, China; 2. College of Mechanical and Electrical Engineering, Anhui Engineering University, Wuhu 241000, China; 3. Tangshan Kaiyuan Welding Automation Technology Institution, Tangshan 063020, China). pp 38 - 42

Abstract: In arc assisted activating TIG welding, the base metal is pre-melted by assisting arc with mixture of argon and oxygen to form an oxide layer, and TIG welding is then carried out, so the weld penetration increases significantly. In this paper, two distribution modes of oxygen on the surface of weld pool was proposed based on experimental measurements, and a more complete model of weld pool in AA-TIG welding was developed. The computed results agreed well with the experimental data and existing theoretical results. Combined with the computed results, Grashof number Gr, magnetic Reynolds number Mm and surface tension Reynolds number Ma were employed to investigate the relative importance of buoyance, Lorentz force and surface tension. Peclet number was use to distinguish the relative intensity of heat convection and heat conduction in the weld pool. The results reveal that the surface tension controlled the flow type of weld pool, and the heat convection determined the heat transfer in weld pool. The relationship between the activating elements and weld penetration during A-TIG welding was clarified.

Key words: oxygen distribution; surface tension; flow; numerical simulation

Simulation of fluid in cylindrical drainage cover for underwater local dry welding LI Lan[1,2], XUE Long[1], HUANG Junfen[1], HUANG Jiqiang[1] (1. Beijing Key Laboratory of Opto-Mechatronic Equipment Technology, Beijing Institute of Petrochemical Technology, Beijing 102617, China; 2. College of Mechanical and Electrical Engineering, Beijing University of Chemical Technology, Beijing 100029, China). pp 43 - 46, 107

Abstract: In underwater local dry welding, the stability of welding procedure is determined by the drainage effect of local drainage device and the turbulence state of fluid in the device, which are two key factors that affect the welding quality. A local drainage device with a cylindrical drain cover structure was developed. Based on fluid mechanics, the simulation was carried out with software FLUENT to explore the drainage process in a circular drainage cover. The influences of different air inlet modes and drainage modes on the phase distribution in the cover and the turbulence state of fluid on the workpiece surface were analyzed. The accuracy of simulation was verified by comparing the simulated drainage process with the experimental one. The results show that the simulated drainage process was consistent with the actual process. Through comparative analysis, the reasonable air inlet and drainage modes for the cylindrical drain cover were determined, and the fundamental data for the stability of underwater local dry welding were provided.

Key words: underwater local dry welding; cylindrical drainage cover; multiphase flow

Dual-beam laser welding and seam tracking control technology for 3D T-beam LIANG Binyan[1], XU Xianyu[2], GONG Shihua[1], WANG Qihang, WANG Xinrun (1. State Engineering Research Center of Manufacturing Equipment Digitization, Huazhong University of Science and Technology, Wuhan 430074, China; 2. Hubei Power Engineering Company, Wuhan 430074, China). pp 47 - 50

Abstract: During dual-beam laser welding of 3D T-beam, the welding structure is complicated and special, the 3D welding path is difficult to fit, and the welding deformation is large. The real-time measurement of 3D T-seam welding was achieved, to solve the mentioned problems, with two laser visual sensors on a Six-axis NC welding machine tool. The actual 3D double-beam welding path was generated using 3D welding path control technology with 3D model of T-seam. Dynamic compensation in dual-beam welding process o f 3D T-seam was achieved using dual-seam real-time closed-loop tracking technology. The actual welding results show that the established dual-beam welding seam tracking technology meets the requirements of dual-beam laser welding.

Key words: 3D T-beam; dual-beam; laser welding; seam tracking

Prediction of reliability of solder joint for fine pitch flip chip assemblies under thermal shock TIAN Ye[1,2], REN Ning[1] (1. School of Mechanical and Electrical Engineering, Henan University of Technology, Zhengzhou 45000, China; 2. School of Materials Science and Engineering, Huazhong University of Science and Technology, Wuhan 430074, China). pp 51 - 54

Abstract: The finite element method was used to analyze the failure of solder joint for fine pitch flip chip assemblies under thermal shock ranging from - 55 to 125 ℃. The fatigue life of critical solders was predicted based on Darveaux lifetime prediction model. The results show that the corner solder failed easiest, and the crack initiated in the solder along the accessory besides the chip, propagating from outside to inside. According to the average crack growth rate and accumulated plastic work density in solder joint, the parameters K_1, K_2, K_3, K_4 for Darveaux lifetime model were calculated to be 1 648.96, - 0.234 9, 0.004 79 and - 0.700 4 respectively, and the predicted fatigue life of the corner solder was 6171 cycles.

Key words: flip chip; micron-solder joint; reliability; fatigue life

Growth analysis of intermetallic compounds on aluminum-steel MIG-brazing interface based on Monte Carlo method LIU Ning[1,2], HUANG Jiankang[1], CHEN Manjiao[1], SHI Yu[1], CAO Rui[1], CHEN Jianhong[1] (1. State Key Laboratory of Advanced Processing and Recycling of Non-ferrous Metals, Lanzhou University of Technology, Lanzhou 730050, China; 2. Baosteel Group Xingjiang Bayi Iron & Steel Co., Ltd., Wulumuqi 830022, China). pp 55 - 58, 62

Abstract: Measurements and analysis with SEM, EDS, XRD confirmed that the intermetallic compounds in aluminum/steel MIG-brazed interface consisted of Fe_2Al_5 and $FeAl_3$ phases. Based on Monte Carlo method, the diffusion of Al and Fe in aluminum/steel interface and growth model for Al-Fe intermetallic compounds were established, and numerical analysis and comparative study were conducted. The results show that the proposed model could well reflect the growth of Fe_2Al_5 phase on steel side, and $FeAl_3$ discretely existed on aluminum side, and the thickness of the intermetallic compound was close to the experimentally measured results.

Key words: aluminum / steel interface; Monte Carlo; intermetallic compound; growth analysis

Super-long life fatigue property of 5A06 aluminum alloy welded joint LI Xiang, DENG Caiyan, GONG Baoming, WANG Dongpo (School of Materials Science and Engineering, Tianjin University, Tianjin 300072, China). pp 59 - 62

(C)1994-2019 China Academic Journal Electronic Publishing House. All rights reserved. http://www.cnki.net